3D HYGRO-MECHANICAL MESO-MODEL FOR WOOD

3D HYGRO-MECHANISCHES MESOMODELL FÜR HOLZ

Serena Gambarelli, Josko Ožbolt

Materials Testing Institute (MPA), University of Stuttgart, Otto-Graf-Institute

SUMMARY

Wood is a fairly complex organic material, which has been in the past widely used not only in many engineering structures but also in cultural heritage objects such as sculptures, paintings, etc. Due to its hygroscopic nature, wood is greatly sensitive to the change of moisture content, mainly induced by variations of air temperature and relative humidity. Exposure of these objects to aggressive environmental conditions, together with mechanical actions, can lead to deterioration and ultimate destruction.

In the present study, a 3D hygro-mechanical meso-scale model for wood is formulated and implemented into the 3D finite element code MASA. The proposed coupled model, consisting of mechanical and non-mechanical part (transport of moisture), is validated against experimental tests available in the literature, confirming its suitability for realistic modeling of wood. The proposed model can be used for the main degradation phenomena (i.e. cracks due to moisture gradients, delamination), which are generated by different environmental and/or mechanical loading conditions. This numerical tool provides useful support for damage analysis of new or existing cultural heritage objects and can help in their preservation.

ZUSAMMENFASSUNG

Holz ist ein ziemlich komplexer organischer Werkstoff, der in der Vergangenheit nicht nur in vielen Ingenieurbauwerken, sondern auch in Objekten des Kulturerbes wie Skulpturen und Gemälden verwendet wurde. Durch seine hygroskopischen Eigenschaften ist Holz recht empfindlich gegenüber Schwankungen der Umgebungstemperatur und der Luftfeuchtigkeit. Wenn Holz solchen angreifenden Umgebungsbedingungen und mechanischen Einwirkungen ausgesetzt wird,

kann dies zu einer Schädigung und zu einer Beeinträchtigung der Dauerhaftigkeit führen.

In der vorliegenden Studie wird ein hygro-mechanisches 3D-Mesomodell für Holz formuliert und in den 3D Finite-Element-Code MASA implementiert. Das vorgeschlagene gekoppelte Modell, das aus einem mechanischen und einem nicht-mechanischen Teil (Feuchtetransport) besteht, wird anhand von in der Literatur verfügbaren experimentellen Tests validiert, wodurch seine Eignung für eine realistische Modellierung von Holz bestätigt wird. Das vorgeschlagene Modell kann für die wichtigsten Degradationsphänomene (d.h. Risse durch Feuchtigkeitsgradienten, Delamination) verwendet werden, die durch unterschiedliche Umwelt- oder mechanische Belastungsbedingungen hervorgerufen werden. Dieses numerische Werkzeug ist eine nützliche Unterstützung bei der Schadensanalyse von neuen oder bestehenden Objekten des kulturellen Erbes und kann zu deren Erhaltung beitragen.

1.   INTRODUCTION

Wood is a fiber composite material with strong orthotropic behavior. Its macroscopic properties vary significantly within the tree cross-section, among different species, along the longitudinal direction and due to possible fiber deviations and knots. The reason for these differences is the complex structure of wood observed at lower length scales. The heterogeneity of wood structure at different scales, typically subdivided into hierarchical levels, namely: micro- (cell walls and lumens), meso- (annual rings) and macro-scale (whole cross section), greatly influences its hygro-thermo-mechanical behavior [1].

The meso-scale structure of wood in the radial (R) and tangential (T) direction, perpendicular to the tree axis, is constituted by alternating early- and late wood annual rings (concentric path form). Both early- and late-wood are composed by "wood cells", consisting of "cell walls" surrounding the "cell lumens", i.e. the holes with polygonal or quadratic cross-section. The early- and late-wood rings differ in lumen shape and thickness of the cell walls [2].

A reliable hygro-thermo-mechanical model for wood should be able to capture the main mechanical damage and transport processes and their interaction on the micro- and meso-scale. These phenomena greatly influence the macroscopic wood behavior. A number of models can be found in the literature dealing with the fracture behavior of wood [3-9]. Some of them [3] identify the average stress

state of pre-defined areas as criterion for structural failure, by using the so called "mean stress approach". In [4] the orthotropic failure criterion for wood is combined with the elasto-plastic material behavior. The model, further developed in [5], accounts for the brittle failure mechanisms of wood under shear and tensile loads, thorough the formulation of a three-dimensional anisotropic material model in combination with interface elements.

Recently, a multi-surface failure approach for wood was proposed by Lukacevic and co-workers [6-9], based on the definition of failure mechanisms at different length scales.

Wood as a hygroscopic material is highly sensitive to the variation of moisture content, which can lead to changes of physical and mechanical properties (e.g. strength and stiffness). Since the moisture diffusion inside the material is not uniform, due to daily and seasonal changes of the climate conditions, moisture gradients occur with consequent moisture-induced stresses that could lead to cracking. In [10] the non-mechanical processes (moisture transport) of wood are described by the classical single (Fickian) diffusion equation for water vapor. As reported in [11], this assumption is reasonable only at low relative humidity, since the moisture transport in wood is mainly governed by the water vapor diffusion in the cell lumens. However, at higher relative humidity the complex meso-scale structure of wood greatly influences the moisture transport system, which is identified by the coupled diffusion of bound water and water vapor, interacting through sorption [12]. With increasing relative humidity, the sorption process slows down [12], while the bound water diffusion in the cell walls becomes more important. This phenomenon, also known as "non-Fickian behavior", cannot be correctly represented by a single-diffusion equation [12]. The multi-Fickian moisture transport model proposed in Frandsen et al. 2007 [12] was validated against experimental data and further extended to account for the hysteretic moisture behavior of wood [13, 14].

Recently, the hygro-thermal behavior of wooden bridge members exposed to realistic climatic conditions was investigated by Fortino et al. 2019 [15]. The influence of the moisture (and possibly heat) distribution on the macroscopic mechanical behavior of wood (hygro-thermo-mechanical model) was investigated by several authors [16, 17].

In the present study, a 3D hygro-mechanical meso-scale model for wood is formulated and implemented into the 3D finite element (FE) code MASA [18]. The non-mechanical part of the model is based on the multi-Fickian moisture transport model [12]. The mechanical part of the model is based on the microplane theory [19], which accounts for initial as well as damage induced anisotropy. The mechanical and non-mechanical parts of the model and their coupling are validated against experimental tests available in the literature [20, 21], confirming the suitability of the approach. The novelty of the here proposed model is the coupling of the microplane-based mechanical model, with the multi-Fickian moisture transport formulation [12]. The model can easily account for the influence of the meso-scale structure of wood in both non-mechanical part (coupled moisture transport model with hysteresis, orthotropic diffusivity) and mechanical part (orientation, width and stiffness of annual rings, non-linear orthotropic behavior), while preserving the macroscopic approach of the FE discretization.

The paper is organized as follows. The mathematical formulation of mechanical and non-mechanical part of the model, as well as their coupling, is presented in Section 2. The numerical results obtained from the 3D FE simulations are discussed in Section 3, based on the comparison with the experimental data available in the literature. Finally, the main conclusions are given in Section 4.

2. FORMULTION OF THE MODEL

2.1 Mechanical model for wood

The mechanical part of the model for wood, originally proposed in [22], is based on the microplane theory [19]. The approach accounts for the initial as well as damage induced anisotropy. In the present study, the model [22] was further developed to realistically capture the complex hygro-mechanical behavior of wood. The employed FE discretization method is based on the definition of two coordinate systems, global and local. The global defines the orientation of annual rings (Fig. 1) and the FE discretization is performed in the local system. In contrary to meso-scale models with discrete modeling of rings, for the given ring width the model automatically recognizes the position of individual rings in the FE mesh. In particular, based on the position of the specimen in the radial (R) – tangential (T) plane, perpendicular to the tree axis, it is possible to determine the orientation of the rings (Fig. 1), which greatly influences the damage mechanisms in wood.
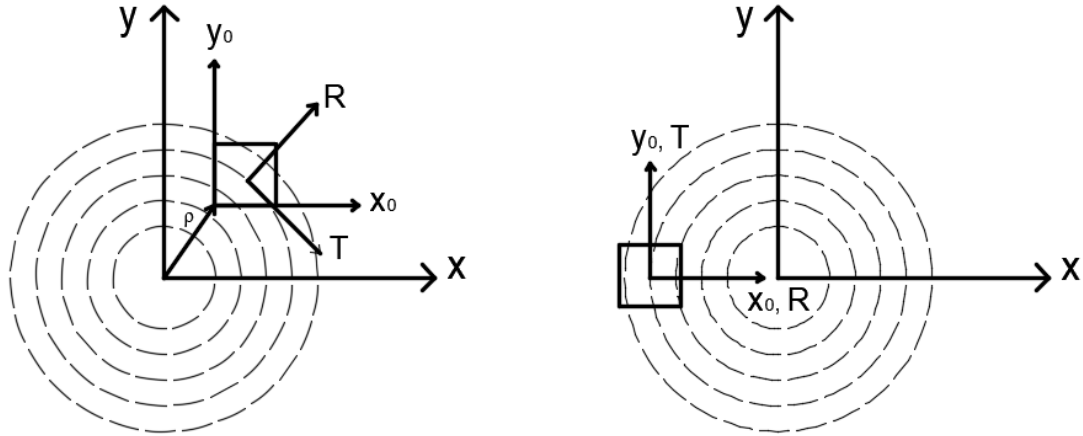
Fig. 1: Position of the specimen in the radial (R) - tangential (T) cross-section of a tree

The initial anisotropy is accounted for through two contributions: (i) initial anisotropy of the microplane model (see [19]) and (ii) high strength of the wood in longitudinal (fiber) direction, where the microplane model is coupled with 1D elastic-brittle constitutive law assuming strain compatibility. This second contribution is the main novelty of the new mechanical model for wood with respect to that proposed in [21], which simplifies the calibration of the material model with respect to the strengths in the three dominant directions of wood (radial, tangential and longitudinal).

The microplane stress-strain relationships are principally the same as formulated for concrete (see [19]) and in case of virgin loading they are based on the scalar damage theory. In the framework of the here proposed meso-scale modeling approach for wood, a suitable bi-linear function κ is introduced to account for the fact that the stiffness and strength of early-wood is approximately three times lower [23] than that of late-wood. To account for the differences in their mechanical properties, the microplane initial stifnesses (volumetric, deviatoric and shear) are multiplied with the bi-linear function κ:

$$C_V = E_{V,0}\kappa(1 - \omega_V) \tag{1a}$$

$$C_D = E_{D,0}\kappa(1 - \omega_D) \tag{1b}$$

$$C_T = E_{T,0}\kappa(1 - \omega_T) \tag{1c}$$

In the microplane model the strength is linear proportional to the initial stiffness parameters of the model, i.e. three times higher initial stiffness of late-wood results in its three times higher strength. Depending on the position of the finite element in the global coordinate system (x, y) the model automatically recognizes the differences between early- and late-wood. It is worth mentioning that the microplane parameters are calibrated based on the properties of the early-wood and the effect of late-wood in the analysis is then accounted for through function κ at the meso-scale.

2.2 *Multi-Fickian moisture transport model for wood*

The non-mechanical part of the proposed model accounts for the coupled moisture transport in wood below the fiber saturation point, characterized by separate transport of water vapor and bound water, interacting through sorption. Due to the variations of the ambient relative humidity, the moisture transport is influenced by the following processes: (1) diffusion of water vapor in wood, (2) sorption of bound water and (3) consequent bound water diffusion. The equations governing the coupled transport of moisture in wood, as formulated in [12], are reported in Appendix A, and the involved parameters/functions are listed in Appendix B (see [12]).

One important aspect influencing the moisture uptake and distribution inside the wood is the definition of the environmental boundary conditions for water vapor (Eq. 2a) and bound water (Eq. 2b):

$$\boldsymbol{n}J_v = \beta_{hum}(h_s - h_{env}) \tag{2a}$$

$$\boldsymbol{n}J_b = 0 \tag{2b}$$

where $\boldsymbol{n}$ is the normal to the surface, J_v and J_b are the moisture fluxes perpendicular to the surface, β_{hum} [ms^{-1}] is the surface moisture transfer coefficient, h_s is the value of relative humidity at the exposed surface and h_{env} is the given relative humidity of the ambient air. Equation (3a) describes the exchange of relative humidity between the wooden surface (h_s) and the surrounding ambient (h_{env}), through the surface transfer coefficient (β_{hum}). At higher air velocities the resistance to diffusion at the surface can be neglected, i.e. the surface relative humidity can be assumed to be identical to the ambient relative humidity ($h_s = h_{env}$) [12]. Since diffusion of the bound water can only take place inside wood

through sorption, there is no transfer through the surface (Eq. 2b), i.e. the flux of bound water normal to the surface is equal to zero.

For the finite element analysis the strong form of mass conservation equations for the two phases (see Appendix A) should be rewritten into the weak form. Because the boundary conditions are given in terms of relative pore pressure (h) the transport of water vapor and bound water is calculated in terms of relative pore pressure ($h = p/p_{sat}$), where p_{sat} [Pa] is the saturation vapor pressure. Note that h and the concentration of water c [kg of water /m³ of wood] for the two phases, are related through sorption curves. The weak form is carried out by employing the Galerkin weighted residual method as (Voigt notation):

$$[C_v]\left\{\frac{\partial h_v}{\partial t}\right\} + [K_v]\{h_v\} = [F_v] \tag{3a}$$

$$[C_b]\left\{\frac{\partial h_b}{\partial t}\right\} + [K_b]\{h_b\} = [F_b] \tag{3b}$$

for the vapor-water (Eq. 7a):

$$[C_v] = \int_V \rho_0 \frac{\partial w_v}{\partial h_v}[N]^T[N]dV$$

$$[K_v] = \int_V \left(\frac{p_{sat}}{RT}\right)[N]^T[D_v][N]dV + \int_S \beta_{hum}[N]^T[N]dS \tag{4a}$$

$$[F_v] = \int_S [N]^T\beta_{hum}h_{env}dS - \int_V [N]^T\dot{c}dV$$

and for the bound water (Eq. 7b):

$$[C_b] = \int_V \rho_0 \frac{\partial w_b}{\partial h_b}[N]^T[N]dV$$

$$[K_b] = \int_V \rho_0 \frac{\partial w_b}{\partial h_b}[N]^T[D_b][N]dV \tag{4b}$$

$$[F_b] = \int_V [N]^T\dot{c}dV$$

in which $w_b = c_b / \rho_0$ and $w_v = c_v / \rho_0$ are respectively the dry moisture contents for bound water and water vapor [kg of water / kg of dry wood], D_b and D_v [m^2/s] are the orthotropic diffusion tensors for the two phases (see Appendix A) and $\dot{c}$ is the sorption rate [kg/(m^3 s)]. The matrix $[N]$ is the column matrix of shape functions, S is the wood surface exposed to environmental conditions, V is the volume of the solid, R is the gas constant of water vapor [J/(kg · K)] and T is the temperature [K].

In the transient FE analysis Eqs. (7a, b) are solved using direct integration of implicit type. The initial conditions for h_v and h_b are determined from the corresponding sorption curves assuming initial equilibrium between the specimen and the ambient relative humidity $(h_v = h_b = h_{env})$ with $\dot{c} = 0$. Therefore, Eqs. 3a, b are separately solved by using the boundary conditions in Eqs. (2a, b). Based on this initial condition, at each time step of the analysis the sorption term $[\dot{c} \neq 0]$ is calculated (see Appendix A) based on h_v and h_b obtained from the previous step and used to evaluate the current h_v and h_b (Eq. 3a, b). In the analysis the driving potentials are not in equilibrium due to the phase change between water vapor and bound water $[\dot{c} \neq 0]$. As shown in section 3.2, only when the equilibrium is approached at high relative humidity, sorption slows down to zero.

2.3   Hygro-mechanical coupling

The governing equation for the mechanical behavior of solids for quasi-static loading condition and assuming standard local Boltzmann continuum reads:

$$\nabla[R_m(u, \theta_w, T)\nabla u] + b = 0 \tag{5}$$

in which R_m is the material stiffness tensor, b is the specific volume load and u is the displacement field. In the mechanical part of the model the total strain tensor (ε_{tot}) is split into mechanical part, elastic (ε_{el}) and damage (ε_{dam}) strains (microplane constitutive law), and non-mechanical part, e.g. hygro-strain due to swelling/shrinkage (ε_{hyg}):

$$\varepsilon_{tot} = \varepsilon_{el} + \varepsilon_{dam} + \varepsilon_{hyg} \tag{6}$$

The swelling and shrinkage strains are calculated based on the dry moisture distribution $(w_b = c_b/\rho_0)$ obtained from the non-mechanical part of the model:

$$\varepsilon_{hyg}(w_b) = \underline{\beta}(w_b - w_{b,ref}) \tag{7}$$

where $w_{b,ref}$ is the reference moisture at the initial state and $\underline{\beta} = [\beta_r; \beta_t; \beta_l; 0; 0; 0]^T$ contains the shrinkage/expansion coefficients for the three material directions.

Coupling between mechanical and non-mechanical part of the model is performed by continuous update of the governing parameters of the incremental transient finite element analysis using staggered solution scheme, i.e. in each time step Δt, the partial differential equation for transport of moisture and the equilibrium equation (mechanical part of the model) are solved simultaneously. This implies that in the mechanical part of the analysis the non-mechanical properties of wood are assumed to be constant and vice versa. The results obtained with the coupled model are reported in a previous publication from the authors [24].

3.   MODEL VALIDATION

3.1   Mechanical model

The mechanical part of the model was validated against the experimental tests performed by Dill-Langer et al. 2002 [20]. The aim of the study was to investigate the crack propagation in the radial (R) – tangential (T) growth plane of soft-wood (spruce) loaded in tension. A total number of 30 pre-notched specimens (60 x 42 x 10 mm^3) were tested in tension, by considering three different configurations for the orientation of the rings with respect to the load direction: RT rings orthogonal to the load direction; TR rings parallel to the load direction; RT45 with angle of 45° between radial and load direction (Fig. 2). The mean annual ring width varied between 1.0 mm for RT specimens to 2.5 mm for TR and RT45. The tested specimens (12 mm length) presented a one-sided initial notch of 0.2 to 0.5 mm length at mid-length (Fig. 2).

The finite element discretization of the sample with notch of 0.5 mm (see Fig. 3) was performed using one-layer 3D eight node solid elements assuming plain strain. A total number of 885 elements were used to discretize the wooden specimen, with average element size of 0.3 mm. The complete FE model counts 1007 solid elements. The thickness of the rings was set as: 2.5 mm for RT45, 1.8 mm for RT and 3.2 mm for TR.
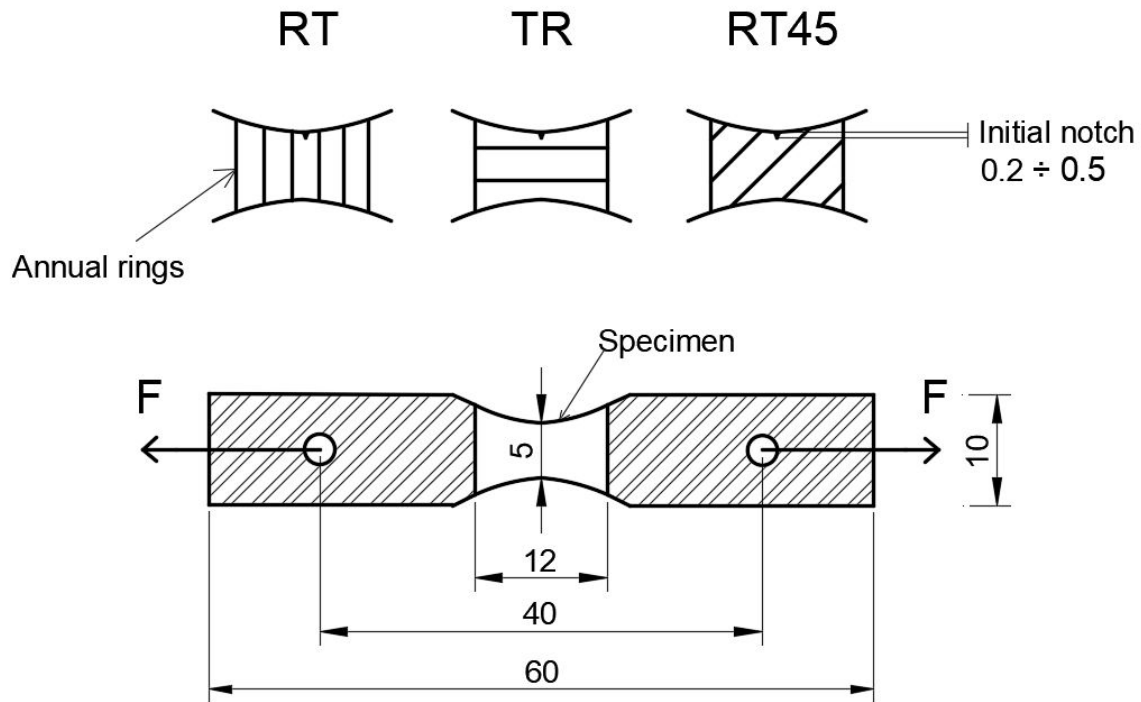
Fig. 2: Notched tension specimen with schematic view of the three considered load/annual ring configurations (dimensions in mm)

The initial macroscopic elasticity moduli and tensile strengths used in the model for early-wood are shown in Table 1 for the three material directions (R,T,L). It is worth mentioning that such properties were determined on the single unit size finite element (microplane model) in radial, tangential and longitudinal directions by trial and error, in order to fit the macroscopic response of the pre-notched test specimen (Figs. 3, 4, 5). Note that only the properties in the radial (R) and tangential (T) direction are relevant to the uniaxial tensile test in the R-T plane. However, the model can well capture the much higher strength/stiffness of the material in the longitudinal (L) direction (Table 1).

Table 1: Initial macroscopic elasticity moduli [MPa] and tensile strengths [MPa] in the three material directions

Moduli of elasticity (microplane – early-wood)			Tensile strength (microplane – early-wood)		
E_R	E_T	E_L	$f_{t,R}$	$f_{t,T}$	$f_{t,L}$
875	590	7000	2.0	1.1	40

The numerical and experimental results for RT45, RT and TR samples, in terms of load-displacement curve and damage evolution, are shown in Figs. 3, 4, 5. A relatively good agreement between numerical and experimental results can be observed for all the analyzed cases. The mechanical model is able to correctly reproduce the uniaxial tensile stress displacement curves for the three considered orientations of the rings (Figs. 3a, 4a, 5a). The crack patterns (Figs. 3b, 4b, 5b), plotted in terms of maximum principal strains and corresponding to a crack opening of 0.1 mm or greater, are also consistent with those observed in the experiments.

a)

b)
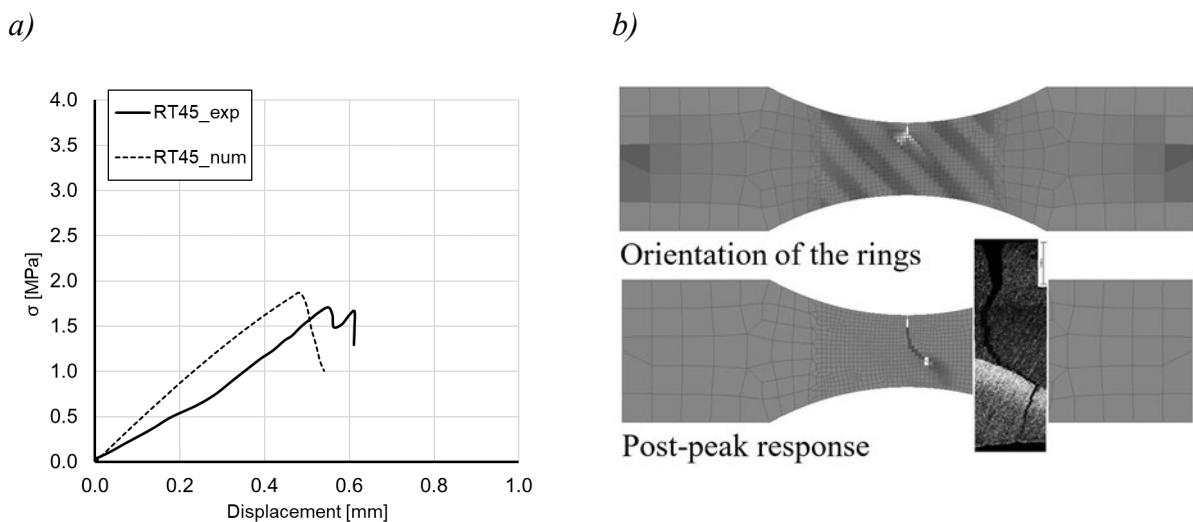
Fig. 3: Wooden specimen (RT45) under uniaxial tension: (a) load-displacement curve; (b) damage evolution (maximum principal strains)

a)

b)
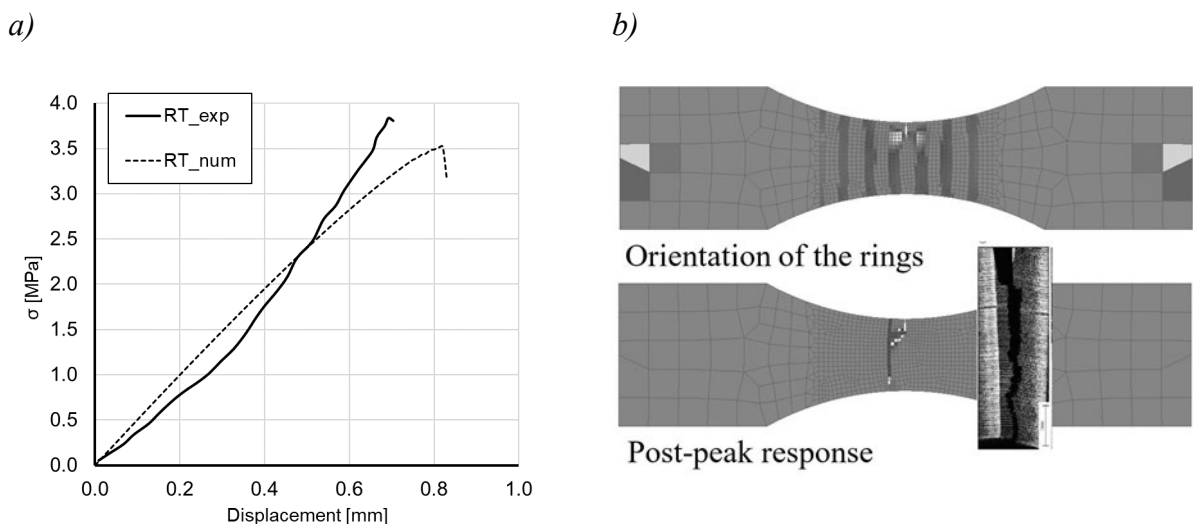
Fig. 4: Wooden specimen (RT) under uniaxial tension: (a) load-displacement curve; (b) damage evolution (maximum principal strains)

a)

b)

Orientation of the rings

Post-peak response
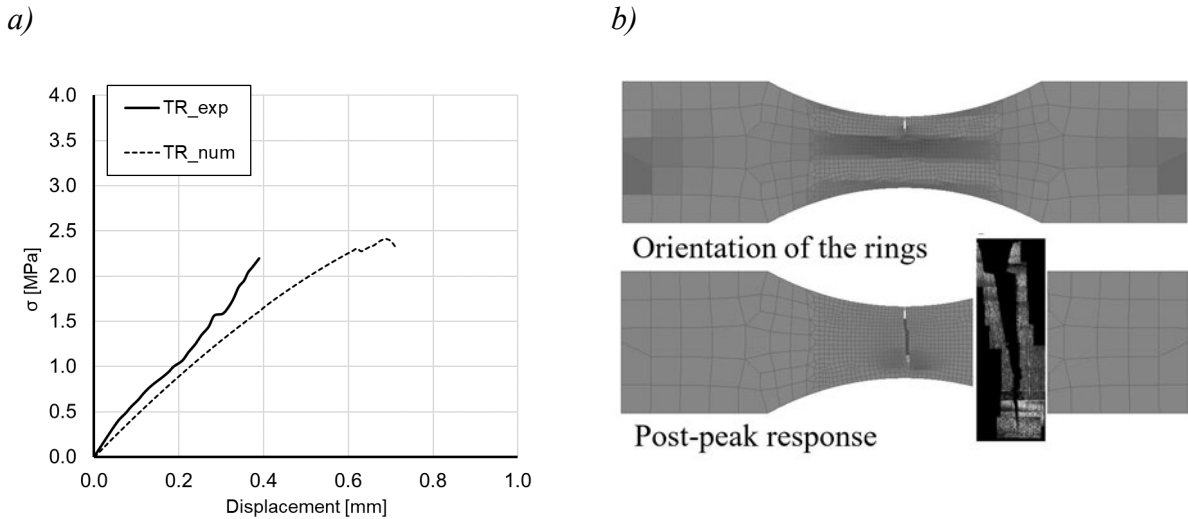
Fig. 5: Wooden specimen (TR) under uniaxial tension: (a) load-displacement curve;
(b) damage evolution (maximum principal strains)

The numerical and experimental tensile strengths are compared in Table 2. It is seen (Table 2) that the ratio between tangential and radial tensile strength $(f_{t,R}/f_{t,T} = 1.8)$ at the element level, corresponds to the ratio of 1.45 (1.73 from the experiments) at the tension test specimen level. In addition to the mechanical properties, the following model parameters influence the macroscopic material behavior: (i) the expression for the function $\Omega(\boldsymbol{n})$ defining the initial anisotropy of the material (microplane); (ii) the assumed bi-linear function $\boldsymbol{\kappa}$, accounting for the lower stiffness of the early-wood with respect to that of late-wood; (iii) the configuration of the rings (width, curvature) and their position with respect to the notch.

Table 2: Experimental and numerical tensile strength [MPa] of the wooden specimen

Experimental		Numerical	
$f_{t,R}$	$f_{t,T}$	$f_{t,R}$	$f_{t,T}$
3.8	2.2	3.5	2.4

3.2   Multi-Fickian moisture transport model

The non-mechanical part of the model was validated against the experimental tests carried out by Wädso et al. (1994a) [21]. In the experiments, transient sorption measurements were carried out on different wooden samples by recording the weight change of the samples as a consequence of an abrupt increase in relative humidity (RH), starting from an initial RH with which the samples were in equilibrium. In particular, two instantaneous steps of relative humidity were numerically analyzed: step B (from 54% to 75%) and step C (from 75% to 84%). The aim was to check whether the model is able to correctly reproduce the non-uniform distribution inside the wood and to capture the non-Fickian behavior experimentally observed at high relative humidity (step C). The obtained numerical results are also compared with those reported in [12].

Simulation was performed only for the sapwood pine sample, with half thicknesses of 8.1 and 4.9 mm, respectively, under one-directional flow transport in the tangential direction. The dry density (ρ) of the material was chosen based on the values (510÷570 kg/m^3) reported by Wadsö [25]. Such values were measured at 50% of relative humidity [25]; therefore a lower density (400 kg/m^3) was assumed in dry condition. The porosity (n = 0.65) was assumed according to the literature [15]. An important parameter for the non-mechanical analysis is the relation between the ambient relative humidity (RH) and the experimentally measured water content in wood, expressed by the isotherm curves. In the present study, the Hailwood-Horrobin isotherm ($f_1 = 2.22$; $f_2 = 15.7$; $f_3 = -14.0$) reported in [12] was used in the transient sorption tests (Fig. 6).
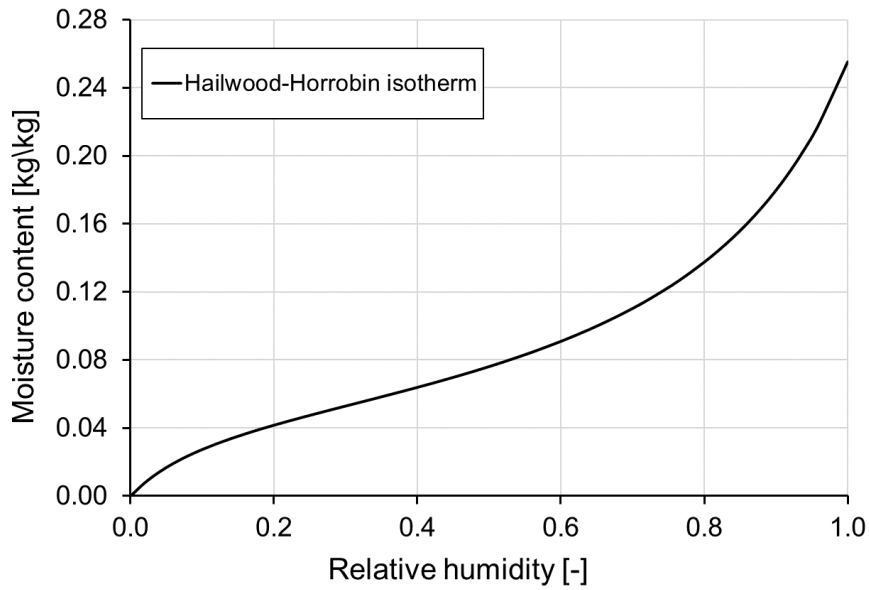
Fig. 6: Adsorption curve for pine

Note that the hysteretic moisture behavior observed due to periodic changes from drying to wetting can be also captured by the model through definition of the scanning curves [14, 26]. They are phenomenological and based on the formulae proposed by Pederson [27]. In the incremental transient FE analysis the model explicitly computes the distribution of relative humidity in the wood and then determines the moisture content based on the sorption curves (see [26]).

The expressions of the orthotropic diffusion tensors for water vapor and bound water are reported in Appendix A. An important aspect for the evaluation of diffusion tensors is the definition of the rings orientation with respect to the global coordinate system (Fig. 1). Suitable formulas, based on the actual orientation of the rings, are implemented in the model for the projection of the diffusion coefficients (radial, tangential and longitudinal direction) in the global coordinate system.

As mentioned above, a mono-directional flow transport in the tangential direction was analyzed for the wooden samples with half thickness of 4.9 and 8.1 mm, respectively. The tangential reduction factor for water vapor and the tangential diffusion coefficient for bound, taken from [12], are summarized in Appendix B. The initial water content is determined from the corresponding sorption curve (Fig. 6) assuming initial equilibrium between the specimen and the ambient relative humidity (54% and 75%, respectively, for the steps B and C). The temperature is kept constant during the analysis and equal to 20°C. The FE discretization and the

environmental boundary conditions for the specimen with half thickness 8.1 mm are shown in Fig. 7. The sample is discretized with 3D eight node solid elements (Fig. 7). However, due to the mono-directional flow transport in the tangential (horizontal) direction, only one layer of elements is modeled in z direction (perpendicular to the specimen plane), while several elements are considered in the vertical (y) direction. Note that for the present case only one row of elements in y direction would also be sufficient.
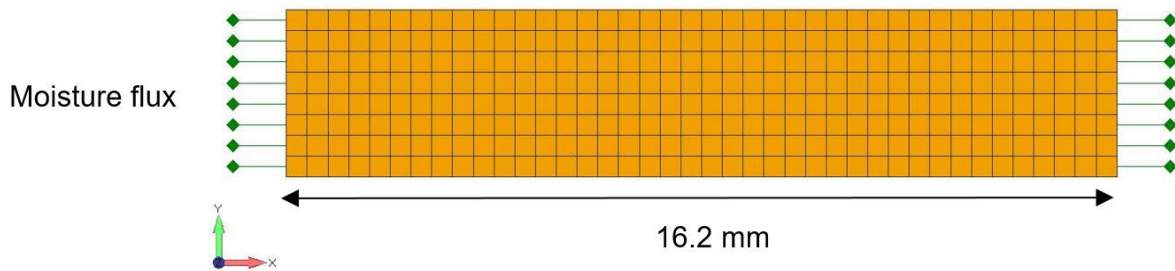
Fig. 7: FE mesh and boundary conditions for the half thickness specimen of 8.1 mm

The environmental boundary conditions are defined for the nodes on the exposed surface, top and bottom. Since in the experiments the air velocity is relatively high (3.0 [ms^{-1}]), the resistance to the vapor transport at the surface humidity is considered negligible ($h_s = h_{env}$). The boundary condition for the bound water it is assumed $\boldsymbol{n}J_b = 0$ (Eq. 2b).

The results of the sorption test are reported in terms of fractional weight increase (E) versus time (t). At each time step, E is evaluated by integrating the bound water concentration over the volume. The experimental and numerical curves for the 8.1 mm half-thick specimen are shown in Fig. 8a for step B and Fig. 8b for step C, respectively. The results from Frandsen et al. 2007 [12] are also included in the graph. A very good agreement between numerical and experimental results is obtained for the step B and slightly larger differences in the first part of the test are observed for the step C. However, the model can correctly capture the reduction of the rate of sorption at higher relative humidity.

a) *b)*
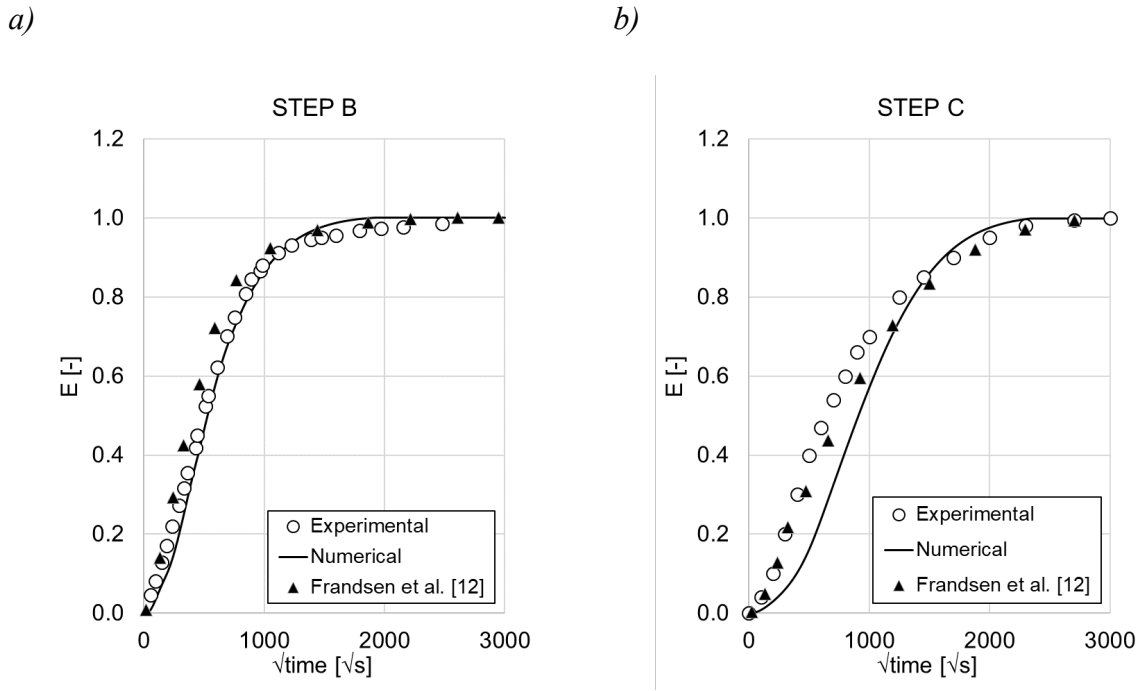
Fig. 8: Numerical vs. experimental moisture curves: (a) step B (54-75%) and (b) step C
(75-84%))

As shown in [21], if the moisture transport is governed by the classical Fick´s law,
the curves obtained for different thicknesses should be the same when plotted as
a function of the square root of time divided by the thickness of the sample.
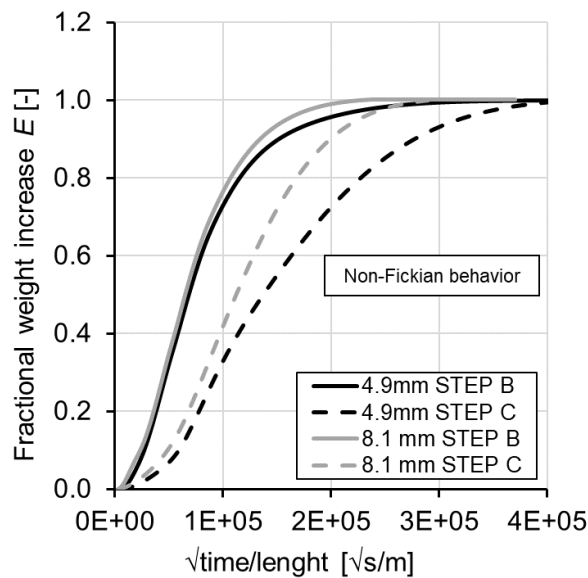
Fig. 9: Variation of fractional weight increase over time for two specimen half thicknesses
(4.9 and 8.1 mm) and two humidity intervals (54-75% and 75-84%)

The obtained numerical results for the two analyzed specimens (half thickness of 4.9 and 8.1 mm) are shown in Fig. 9 for both steps. Similarly as in the experiments, the non-Fickian behavior of wood is observed at high relative humidity (step C) due to fast sorption of the bound water. Furthermore, the curves corresponding to the half-thick specimen of 8.1 mm are to the left of the curves for the thinner sample (half-thickness 4.9 mm).

A comparison between experimental and numerical diffusivities is provided in Table 3. Similarly as in the experiments [21] the diffusivities are calculated from the slope of the sorption curves (Fig. 8):

$$D_c^* = \frac{\pi l^2}{4} \left(\frac{dE}{d\sqrt{t}} \right)^2 \tag{8}$$

where l is the half thickness of the sample, t is the time, and E is the fractional weight change.

Table 3: Experimental and numerical diffusivities

D_c^* 10^{-12} [m²/s]	STEP B	STEP C
Experimental	66±5	33±2
Numerical	77	32

Fig. 10 shows the distribution of water vapor (relative humidity) and bound water (moisture) over the specimen thickness at different time steps of the analysis. It is seen that the model can capture the main features of the coupled transport system. The results are in very good agreement with those obtained in [12] for the same experimental tests (Fig. 10). The applied boundary conditions (Eq. 2a,b) lead to a gradual increase of the moisture gradient close to the boundaries (Fig. 10b), while the relative humidity at the wood surfaces (Fig. 10a) is constant and equal to the imposed ambient relative humidity (75%). This means that during diffusion process the water vapor gradually absorbs into bound water.

a)

b)
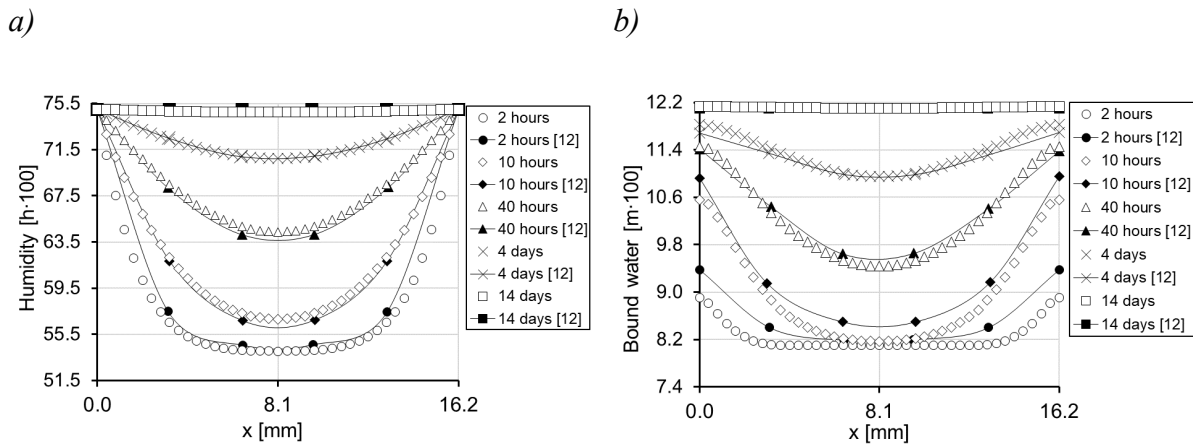
Fig. 10: Distribution of water vapor (relative humidity) (a) and bound water (in terms of moisture content) (b) for 8.1mm specimen in tangential direction (54-75% RH)

With time (14 days), the moisture content of wood comes into equilibrium with the ambient relative humidity (stationary conditions). This moisture content is defined as the equilibrium moisture content (emc) of the wood. The use of the classical single diffusion equation (Fickian model) would overestimate the moisture gradients at the boundaries observed at low ranges of relative humidity (see [10]). The explanation is that the single diffusion equation implies that the moisture transport in wood is governed by water vapor diffusion, with boundary conditions as specified in Eq. (2a). Such model predicts higher and not realistic moisture gradients at the boundaries [10], with possible cracking, even for lower values of relative humidity.

4.   CONCLUSIONS

In the present study, a 3D hygro-mechanical meso-scale model for wood is presented and discussed. The coupled model consists of mechanical and non-mechanical part (transport of moisture). The mechanical behavior of wood is described by the microplane material model, which accounts for the initial as well as damage induced anisotropy. The non-mechanical part of the model is based on the multi-Fickian moisture transport system [12]. The effect of temperature on the moisture distribution is neglected in this study. Both mechanical and non-mechanical parts of the model were implemented into the 3D-FE code MASA and validated against experimental tests. From the obtained results, the following can be concluded: (1) The mechanical part of the model can correctly reproduce the macroscopic behavior of wood subjected to mechanical loads. The novelty of the

model is the use of the microplane theory to account for both the initial and damage-induced anisotropy; (2) Differently to the meso-scale models with discrete modeling of the annual rings, for the given annual ring width and its orientation in the global coordinates, the model recognizes their position in the FE mesh. This is of great advantage in the general 3D FE modeling of wood because the modeling approach (discretization) is the same as in the standard macroscopic FE analysis; however, the FE model automatically recognizes the complex meso-scale structure of wood; (3) It is shown that the mechanical part of the model reasonably well capture the material behavior, both in terms of load-displacement curve and failure mode. Moreover, the non-mechanical model can account for the main features of the multi-Fickian moisture transport.

APPENDIX A (Governing equations of the multi-Fickian moisture transport model [12])

Combined moisture transport of water vapor (c_v) and bound water (c_b) below the fiber saturation point:

$$\frac{\partial c_v}{\partial t} = \nabla(\boldsymbol{D_v}\nabla c_v) - \dot{c} \tag{1a}$$

$$\frac{\partial c_b}{\partial t} = \nabla(\boldsymbol{D_b}\nabla c_b) + \dot{c} \tag{1b}$$

Where c_v and c_b are the concentration of water for water vapor and bound water [kg of water/m³ of wood]. $\dot{c}$ is the coupling sorption term [kg/(m³ s)], respectively. The different sign of $\dot{c}$ in the previous equations indicates the gradual absorption of bound water (negative sign) into bound water (positive sign).

Orthotropic diffusion tensor for the water vapor $\boldsymbol{D_v}$ [m²/s]:

$$\boldsymbol{D_v} = \boldsymbol{\xi^T}\, 2.31\ \text{x}10^{-5}\, \frac{p_{atm}}{p_{atm} + p_v}\left(\frac{T}{273.15}\right)^{1,81} \tag{2}$$

Orthotropic diffusion tensor for the bound water $\boldsymbol{D_b}$ [m²/s]:

$$\boldsymbol{D_b} = \boldsymbol{D}_{0b}\, exp\left(\frac{-E_b(w_b)}{R_u T}\right) \tag{3}$$

Sorption rate $\dot{c}$ [kg/(m³ s)]:

$$\dot{c} = H(p_v - p_b) \tag{4}$$

APPENDIX B (Parameters/functions used in the multi-Fickian moisture transport model [12])

Parameters for $[D_v]$:

Reduction factors for pine $\boldsymbol{\xi}^T = [R = 0.03; T = 0.03; L = 0.9]$

Reduction factors for oak $\boldsymbol{\xi}^T = [R = 0.09; T = 0.09; L = 0.9]$

Atmospheric pressure $[p_{atm}] = 101325$ [Pa]

Water vapor pressure p_v [Pa]

Temperature $[T] = 293.15$ K

Parameters for $[D_b]$:

$\boldsymbol{D_{0b}^T} = [R = 7.0 \text{ x } 10^{-6}; T = 7.0 \text{ x } 10^{-6}; L = 17.5 \text{ x } 10^{-6}]$

Universal gas constant $R_u = 8.314$ [J/(mol $\cdot$ K)]

Activation energy of the bound water $E_b = 38500 - 29000 \, w_b$ [J/mol]

Dry moisture content $w_b = c_b/\rho_0$ [kg of water/ kg of dry wood]

Parameters for $[\dot{c}\,]$:

Reaction rate function:

$$H \text{ [kg/(m}^3 \cdot \text{Pa)]} = \begin{cases} c_1 exp\left(-c_2 \left(\dfrac{p_b}{p_v}\right)^{c_3}\right) + c_4 & ; \, p_b \leq p_v \\[4mm] c_1 exp\left(-c_2 \left(\dfrac{p_b}{p_v}\right)^{-c_3}\right) + c_4 & ; \, p_b > p_v \end{cases}$$

$c_1 = \, 2.60 \text{ x } 10^{-6}$ [kg/(m$^3 \cdot$ Pa)]
$c_2 = 5.22 \text{ x } 10^{-6} \exp(19 h_{env})$
$c_3 = \, 50.0$ [$-$]
$c_4 = \, 8.0 \text{ x } 10^{-8}$ [kg/(m$^3 \cdot$ Pa)]

REFERENCES

[1] Wittel, F.K., Dill-Langer, G., Kröplin, B.H.: *Modeling of damage evolution in soft-wood perpendicular to grain by means of a discrete element approach*, Computational Materials Science, 2005, 32: 594–60

[2] Hofstetter, K., Hellmich, C., Eberhardsteiner, J.: *Development and experimental validation of a continuum micromechanics model for the elasticity of wood*, European Journal of mechanics A/Solids, 2005, 24: 1030-1053

[3] Aicher, S., Gustafsson, PJ., Haller, P., Petersson, H.: *Fracture mechanics models for strength analysis of timber beams with a hole or a notch*, a report of rilem tc-133, 2002

[4] Schmidt, J., Kaliske, M.: *Zur dreidimensionalen Materialmodellierung von Fichtenholz mittels eines Mehrflächen-Plastizitätsmodells*, Holz als Roh- und Werkstoff, 2006, 64: 393–402

[5] Schmidt, J., Kaliske, M.: *Simulation of cracks in wood using a coupled material model for interface elements*, Holzforschung, 2007, 61: 382-389

[6] Lukacevic, M., Füssl, J., Lampert, R.: Failure mechanisms of clear wood identified at wood cell level by an approach based on the extended finite element method, Eng. Fract. Mech., 2015, 144:158-175

[7] Lukacevic, M., Füssl, J.: *Application of multisurface discrete crack model for clear wood taking into account the inherent microstructural characteristics of wood cells*, Holzforschung, 2016, 70(9): 845-853

[8] Lukacevic M., Füssl, J., Eberhardsteiner J.: *A numerical approach to describe failure of wood - From the wood cell level up to wood-based products*, Conference: WCTE 2016 - World Conference on Timber Engineering, Vienna, Austria, 2016

[9] Lukacevic, M., Lederer, W., Füssl, J.: *A microstructure-based multisurface failure criterion for the description of brittle and ductile failure mechanisms of clear wood*, Engineering Fracture Mechanics, 2017, 176: 83-99

[10] FRANKE, B., FRANKE, S., SCHIERE, M., MÜLLER, A.: *Moisture diffusion in wood – Experimental and numerical investigatios*, World Conference on Timber Engineering (WCTE 2016), Vienna, Austria, 2016

[11] KRABBENHØFT, K., DAMKILDE, L.: *A model for non-fickian moisture transfer in wood*, Mater. Struct., 2004, 37: 615-622

[12] FRANDSEN, H.L. DAMKILDE, L., SVENSSON, S.: *A revised multi-Fickian moisture transport model to describe non-Fickian effects in wood*, Holzforschung, 2007, 61: 563-572

[13] FRANDSEN, H.L., SVENSSON, S., DAMKILDE, L.: *A hysteresis model suitable for numerical simulation of moisture content in wood*, Holzforschung 61, 2007: 75-181

[14] FRANDSEN, H.L., SVENSSON, S.: *Implementation of sorption hysteresis in multi-Fickian moisture transport*, Holzforschung 61, 2007: 693-701

[15] FORTINO, S., HRADIL, P., GENOESE, A., GENOESE, A., POUSETTE, A.: *Numerical hygro-thermal analysis of coated wooden bridge members exposed to Northern European climates*, Construction and Building Materials, 2019, 208: 492-505

[16] KONOPKA, D., KALISKE, M.: *Transient multi-Fickian hygro-mechanical analysis of wood*, Computers & structures, 2018, 197: 12-17

[17] AUTENGRUBER, M., LUKACEVIC, M., GRÖSTLINGER, C., FÜSSL, J.: *Finite-element-based prediction of moisture-induced crack patterns for cross sections of solid wood and glued laminated timber exposed to a realistic climate condition*, Const. Build. Mat. 271, 2021, 121775

[18] OŽBOLT, J.: MASA – „*Macroscopic Space Analysis*", Internal Report, Institut für Werkstoffe im Bauwesen, Universität Stuttgart, Germany, 1998

[19] OŽBOLT, J., LI, Y.-J., KOŽAR, I.: *Microplane model for concrete with relaxed kinematic constraint*, International Journal of Solids and Structures, 2001, 38: 2683-2711

[20] Dill-Langer, G., Lütze, S., Aicher, S.: *Microfracture in wood monitored by confocal laser scanning microscopy*, Wood Science and Technology, 2002, 36: 487–499

[21] Wadsö, S.: *Unsteady-state water vapor adsorption in wood: an experimental study*, Wood Fiber Science, 1994a, 26(1): 36-50

[22] Ožbolt, J., Aicher, S.: *Macroscopic modeling of wood using microplane theory*, in: Proc. Int. Conf. on Wood and Wood Fiber Composites, S. Aicher (Ed.), Otto-Graf-Institute, Stuttgart, 2000, 253–264

[23] Dill-Langer, G.: *Schädigung von Brettschichtholz bei Zugbeanspruchung rechtwinklig zur Faserrichtung*, PhD dissertation, Materialprüfungsanstalt Universität Stuttgart, 2004

[24] Gambarelli, S., Ožbolt, J.: *3D hygro-mechanical meso-scale model for wood, Construction and Building Materials*, 311: 125283, 2021.

[25] Wadsö, L.: *An error analysis of the sorption method for woo*d. Part 2. Application, Holzforschung, 48: 133-138, 1994

[26] Ožbolt, J., Oršanić, F., Balabanić, G.: *Modeling influence of hysteretic moisture behavior on distribution of chlorides in concrete*, Cement and Concrete Composites, 2016, 67, 73-84

[27] Pederson, C.R.: *Combined Heat and Moisture Transfer in Building Constructions*, Dissertation, Lyngby, Denmark, 1990